judgment of PSA failure is often difficult and vague with the ASTRO definition, especially when the intervals between measurement are shorter than recommended, which sometimes occurs as a result of a patient's desire to monitor their PSA levels as often as possible. Therefore, we employed the criteria of "nadir plus 2", reported by Coen et al.,[14] with a modification so as not to misinterpret the temporary rise in PSA after the initial treatment as PSA failure. The results with these two definitions matched in 93% of our patient cohort for the judgment of PSA failure; however, time to failure was approximately 6 months shorter with the ASTRO definition.

It is notable that as many as 22% of the patients in our series developed a second primary malignancy; this is significantly higher than the figure reported by Movsas et al.[36] It should be emphasized that none of these malignancies fulfilled the classic definition of radiation-induced malignancy (arising within the radiation field and a minimum 5-year interval between prior radiotherapy and the development of a second malignancy). Considering the high incidence of death from intercurrent disease, including a second primary cancer, less invasive treatment, such as radiation therapy, is a reasonable option for this elderly population.

Based on the results of the present study, we are now undertaking a phase II study with dose escalation to 78 Gy, using IMRT, for patients with stage III disease. The role of adjuvant hormonal therapy following EBRT for Japanese men will be assessed in our next study.

In conclusion, NHT followed by 70 Gy of EBRT, using a dynamic conformal technique, is feasible for Japanese men and produced a favorable survival result. Assessment of the effect of an increased radiation dose and/or the use of adjuvant hormonal therapy is warranted in future studies.

References

1. National Cancer Center (2003) Cancer statistics in Japan 2003
2. Walsh PC (1997) Immediate versus deferred treatment for advanced prostatic cancer: initial results of the Medical Research Council trial. The Medical Research Council Prostate Cancer Working Party Investigators Group. J Urol 158:1623–1624
3. Lundgren R, Nordle O, Josefsson K (1995) Immediate estrogen or estramustine phosphate therapy versus deferred endocrine treatment in nonmetastatic prostate cancer: a randomized multicenter study with 15 years of followup. The South Sweden Prostate Cancer Study Group. J Urol 153:1580–1586
4. Aus G, Adolfsson J, Selli C, et al. (2002) Treatment of patients with clinical T3 prostate cancer. Scand J Urol Nephrol 36:28–33
5. Pilepich MV, Krall JM, al-Sarraf M, et al. (1995) Androgen deprivation with radiation therapy compared with radiation therapy alone for locally advanced prostatic carcinoma: a randomized comparative trial of the Radiation Therapy Oncology Group. Urology 45:616–623
6. Bolla M, Gonzalez D, Warde P, et al. (1997) Improved survival in patients with locally advanced prostate cancer treated with radiotherapy and goserelin. N Engl J Med 337:295–300
7. Pilepich MV, Winter K, John MJ, et al. (2001) Phase III Radiation Therapy Oncology Group (RTOG) trial 86–10 of androgen deprivation adjuvant to definitive radiotherapy in locally advanced carcinoma of the prostate. Int J Radiat Oncol Biol Phys 50:1243–1252
8. Shipley WU, Lu JD, Pilepich MV, et al. (2002) Effect of a short course of neoadjuvant hormonal therapy on the response to subsequent androgen suppression in prostate cancer patients with relapse after radiotherapy: a secondary analysis of the randomized protocol RTOG 86–10. Int J Radiat Oncol Biol Phys 54:1302–1310
9. Oken MM, Creech RH, Tormey DC, et al. (1982) Toxicity and response criteria of the Eastern Cooperative Oncology Group. Am J Clin Oncol 5:649–655
10. Nagata Y, Okajima K, Murata R, et al. (1996) Development of an integrated radiotherapy network system. Int J Radiat Oncol Biol Phys 34:1105–1111
11. Zhu S, Mizowaki T, Nagata Y, et al. (2005) Comparison of three radiotherapy treatment planning protocols of definitive external-beam radiation for localized prostate cancer. Int J Clin Oncol 10:398–404
12. Cox JD, Stetz J, Pajak TF (1995) Toxicity criteria of the Radiation Therapy Oncology Group (RTOG) and the European Organization for Research and Treatment of Cancer (EORTC). Int J Radiat Oncol Biol Phys 31:1341–1346
13. American Society for Therapeutic Radiology and Oncology consensus panel (1997) Consensus statement: guidelines for PSA following radiation therapy. American Society for Therapeutic Radiology and Oncology Consensus Panel. Int J Radiat Oncol Biol Phys 37:1035–1041
14. Coen JJ, Chung CS, Shipley WU, et al. (2003) Influence of follow-up bias on PSA failure after external beam radiotherapy for localized prostate cancer: results from a 10-year cohort analysis. Int J Radiat Oncol Biol Phys 57:621–628
15. D'Amico AV, Whittington R, Kaplan I, et al. (1997) Equivalent biochemical failure-free survival after external beam radiation therapy or radical prostatectomy in patients with a pretreatment prostate specific antigen of >4–20 ng/ml. Int J Radiat Oncol Biol Phys 37:1053–1058
16. Keyser D, Kupelian PA, Zippe CD, et al. (1997) Stage T1–2 prostate cancer with pretreatment prostate-specific antigen level < or = 10 ng/ml: radiation therapy or surgery? Int J Radiat Oncol Biol Phys 38:723–729
17. Kupelian P, Katcher J, Levin H, et al. (1997) External beam radiotherapy versus radical prostatectomy for clinical stage T1–2 prostate cancer: therapeutic implications of stratification by pretreatment PSA levels and biopsy Gleason scores. Cancer J Sci Am 3:78–87
18. Sato K, Tsuchiya N, Habuchi T, et al. (2003) Total cystoprostatectomy in the treatment of locally advanced prostate carcinoma. Aktuelle Urol.34:259–261
19. Kanamaru H, Arai Y, Akino H, et al. (1999) Long-term treatment results of elderly patients with prostate cancer in Japan: an analysis of prognostic factors. Jpn J Clin Oncol 29:151–155
20. Gerber GS, Thisted RA, Chodak GW, et al. (1997) Results of radical prostatectomy in men with locally advanced prostate cancer: multi-institutional pooled analysis. Eur Urol 32:385–390
21. van den Ouden D, Hop WC, Schroder FH (1998) Progression in and survival of patients with locally advanced prostate cancer (T3) treated with radical prostatectomy as monotherapy. J Urol 160:1392–1397
22. Akakura K, Isaka S, Akimoto S, et al. (1999) Long-term results of a randomized trial for the treatment of stages B2 and C prostate cancer: radical prostatectomy versus external beam radiation therapy with a common endocrine therapy in both modalities. Urology 54:313–318
23. Valicenti R, Lu J, Pilepich M, et al. (2000) Survival advantage from higher-dose radiation therapy for clinically localized prostate cancer treated on the Radiation Therapy Oncology Group trials. J Clin Oncol 18:2740–2746
24. Kupelian PA, Elshaikh M, Reddy CA, et al. (2002) Comparison of the efficacy of local therapies for localized prostate cancer in the prostate-specific antigen era: a large single-institution experience with radical prostatectomy and external-beam radiotherapy. J Clin Oncol 20:3376–3385
25. Pollack A, Zagars GK, Starkschal, G, et al. (2002) Prostate cancer radiation dose response: results of the M. D. Anderson phase III randomized trial. Int J Radiat Oncol Biol Phys 53:1097–1105
26. Laverdiere J, Nabid A, De Bedoya LD, et al. (2004) The efficacy and sequencing of a short course of androgen suppression on free-

dom from biochemical failure when administered with radiation therapy for T2-T3 prostate cancer. J Urol 171:1137–1140
27. Laverdiere J, Gomez JL, Cusan L, et al. (1997) Beneficial effect of combination hormonal therapy administered prior and following external beam radiation therapy in localized prostate cancer. Int J Radiat Oncol Biol Phys 37:247–252
28. Forman JD, Kumar R, Haas G, et al. (1995) Neoadjuvant hormonal downsizing of localized carcinoma of the prostate: effects on the volume of normal tissue irradiation. Cancer Invest 13:8–15
29. Liu M, Pickles T, Agranovich A, et al. (2004) Impact of neoadjuvant androgen ablation and other factors on late toxicity after external beam prostate radiotherapy. Int J Radiat Oncol Biol Phys 58:9–67
30. Sanguineti G, Agostinelli S, Foppiano F, et al. (2002) Adjuvant androgen deprivation impacts late rectal toxicity after conformal radiotherapy of prostate carcinoma. Br J Cancer 86:1843–1847
31. Valicenti RK, Winter K, Cox JD, et al. (2003) RTOG 94-06: is the addition of neoadjuvant hormonal therapy to dose-escalated 3D conformal radiation therapy for prostate cancer associated with treatment toxicity? Int J Radiat Oncol Biol Phys 57:614–620
32. Pilepich MV, Caplan R, Byhardt RW, et al. (1997) Phase III trial of androgen suppression using goserelin in unfavorable-prognosis carcinoma of the prostate treated with definitive radiotherapy: report of Radiation Therapy Oncology Group Protocol 85–31. J Clin Oncol 15:1013–1021
33. Roach M 3rd, Lu J, Pilepich MV, et al. (2000) Predicting long-term survival, and the need for hormonal therapy: a meta-analysis of RTOG prostate cancer trials. Int J Radiat Oncol Biol Phys 47:617–627
34. Zelefsky MJ, Fuks Z, Hunt M, et al. (2001) High dose radiation delivered by intensity modulated conformal radiotherapy improves the outcome of localized prostate cancer. J Urol 166:876–881
35. Roach M 3rd, DeSilvio M, Lawton C, et al. (2003) Phase III trial comparing whole-pelvic versus prostate-only radiotherapy and neoadjuvant versus adjuvant combined androgen suppression: Radiation Therapy Oncology Group 9413. J Clin Oncol 21:1904–1911
36. Movsas B, Hanlon AL, Pinover W, et al. (1998) Is there an increased risk of second primaries following prostate irradiation? Int J Radiat Oncol Biol Phys 41:251–255

Diffusion-Tensor Fiber Tractography: Intraindividual Comparison of 3.0-T and 1.5-T MR Imaging[1]

Tsutomu Okada, MD
Yukio Miki, MD, PhD
Yasutaka Fushimi, MD
Takashi Hanakawa, MD, PhD
Mitsunori Kanagaki, MD, PhD
Akira Yamamoto, MD
Shin-ichi Urayama, PhD
Hidenao Fukuyama, MD, PhD
Masahiro Hiraoka, MD, PhD
Kaori Togashi, MD, PhD

Purpose: To prospectively evaluate the depiction of brain fiber tracts at 3.0- versus 1.5-T diffusion-tensor (DT) fiber tractography performed with parallel imaging.

Materials and Methods: Institutional review board approval was obtained, and each subject provided written informed consent. Subjects were 30 healthy volunteers (15 men, 15 women; mean age, 28 years; age range, 21–46 years). Single-shot spin-echo echo-planar magnetic resonance (MR) sequences with parallel imaging were applied. Four fiber tracts were reconstructed: corticospinal tract (CST), superior longitudinal fasciculus (SLF), corpus callosum (CC), and fornix. Two neuroradiologists compared 3.0- and 1.5-T tractography in terms of fiber tract depiction by using five depiction scores (scores 0–4) and numbers of reconstructed tract fibers and in terms of lateral asymmetry in the CST by using numbers of reconstructed fibers. The Wilcoxon signed rank test was applied for statistical analysis.

Results: Visual scores for both CST hemispheres ($P < .001$), the right SLF ($P = .005$), the CC ($P = .01$), and the right fornix ($P = .04$) were higher at 3.0-T DT tractography. Larger numbers of CST (right, $P = .008$; left, $P < .001$), SLF (right, $P = .001$; left, $P = .02$), and fornix (bilaterally, $P = .02$) tract fibers were depicted at 3.0 T. The asymmetry index for the CST was lower ($P < .001$) at 3.0 T. Visual scores for the left SLF and the left fornix and numbers of CC tract fibers were not significantly different.

Conclusion: Depiction of most fiber tracts was improved at 3.0-T DT tractography compared with depiction at 1.5-T tractography.

[1] From the Department of Diagnostic Imaging and Nuclear Medicine (T.O., Y.M., Y.F., M.K., A.Y., K.T.) and Department of Therapeutic Radiology and Oncology (M.H.), Graduate School of Medicine, and Human Brain Research Center (T.H., S.U., H.F.), Kyoto University, 54 Kawahara-cho, Shogoin, Sakyo-ku, Kyoto-shi, Kyoto 606-8507, Japan. From the 2004 RSNA Annual Meeting. Received December 30, 2004; revision requested March 17, 2005; revision received May 4; final version accepted June 1. Supported in part by grants from the Ministry of Health, Labor and Welfare of Japan (k0800006-01) and the Ministry of Education Culture, Sports, Science and Technology of Japan (C)(15591270).

Diffusion-tensor (DT) imaging is a magnetic resonance (MR) imaging technique that is sensitive to the orientation of mobility in intravoxel water molecules (1,2). DT imaging reveals two specific characteristics: diffusion anisotropy and the directional distribution of water diffusivity. When water diffusion in a tissue is almost the same in all directions, the diffusion is considered to be isotropic and have lower anisotropy. Conversely, when water diffusion is restricted along a specific direction, the diffusion is considered to be anisotropic and have higher anisotropy. Brain white matter has high diffusion anisotropy because diffusion is faster when it is parallel to the fiber direction than when it is the same in all other directions (3,4).

DT images of the human brain can be reconstructed for visualization of the macroscopic three-dimensional fiber tract architecture by using a process known as fiber tractography, or the fiber-tracking technique (5–10). DT imaging and fiber tractography are powerful tools for studying cerebral white matter and have been applied clinically to assess brain tumors (11,12), diffuse axonal injury (13), pediatric brain development (14), and cerebral infarcts (15).

With recent advances in actively shielded 3.0-T magnets, the use of high-field-strength MR imaging in clinical settings has become practical (16,17). Parallel imaging techniques, such as simultaneous acquisition of spatial harmonics, or SMASH (18); sensitivity encoding (19); and auto-SMASH–based generalized autocalibrating partially parallel acquisition (20), also have improved with recent advances in MR imaging hardware. Owing to shortened echo train lengths and echo times, parallel imaging techniques can be used to reduce artifacts related to spin-echo echo-planar imaging. Some reports have described the performance of parallel imaging in spin-echo echo-planar DT imaging and fiber tractography at 1.5 or 3.0 T (9,10,21–24). However, to our knowledge, in no reports have the differences between 3.0- and 1.5-T spin-echo echo-planar DT fiber tractography with parallel imaging been compared. Thus, the purpose of our study was to prospectively evaluate the depiction of brain fiber tracts at 3.0-T versus 1.5-T DT fiber tractography performed with parallel imaging.

Materials and Methods

Study Subjects

The study population comprised 30 healthy volunteers (15 men, 15 women; mean age, 28 years; age range, 21–46 years) with no history of neurologic injury or psychiatric disease. All subjects were examined by one of the authors (T.H., with 14 years of experience as a neurologist), and no subjects had abnormal neurologic signs or symptoms. Institutional review board approval was obtained for this study, and each subject provided written informed consent.

Data Acquisition

All subjects underwent 3.0- and 1.5-T DT imaging, which was performed by using a whole-body 3.0-T MR unit (Trio; Siemens, Erlangen, Germany) with a 40 mT/m gradient and a 1.5-T MR unit (Symphony; Siemens) with a 30 mT/m gradient, on the same day. MR imaging at 3.0 T was performed by one author (T.O.), and MR imaging at 1.5 T was performed by another author (Y.F.), both of whom had 8 years of experience as neuroradiologists and 2 years of experience in DT imaging. The time delay between 3.0- and 1.5-T MR imaging was less than 1 hour for all subjects. Both MR units were equipped with integrated parallel acquisition capability and a receive-only eight-channel phased-array head coil. Both the 3.0-T and the 1.5-T DT imaging examinations involved the use of single-shot spin-echo echo-planar sequences and nearly identical parameters: 5200/79 (repetition time msec/echo time msec), a 220-mm field of view, a 128 × 128 matrix, 3-mm section thickness without intersection gaps (matrix size, 1.7 × 1.7 × 3.0 mm), and four repetitions.

The generalized autocalibrating partially parallel acquisition algorithm was applied for parallel imaging with use of a reduction factor of two, 24 additional autocalibrating phase-encoding steps in the center of k-space, and a 75% partial Fourier technique in the phase-encoding direction. Only the bandwidths differed: A bandwidth of 1502 Hz per pixel was used for 3.0-T imaging, and a bandwidth of 1056 Hz per pixel was used for 1.5-T imaging. Motion-probing gradients were applied along 12 noncolinear directions with a b factor of 700 sec/mm^2 after one non–diffusion-weighted image (b = 0 sec/mm^2) was obtained. A total of 40 sections encompassed the entire cerebral hemisphere and the brainstem. The imaging times for 3.0- and 1.5-T DT imaging were almost the same—about 7.5 minutes.

Data Processing

DT imaging data sets were transferred, in Digital Imaging and Communications in Medicine format, to a Windows personal computer (IBM, New York, NY) workstation. DtiStudio, version 1.02, software (H. Jiang, S. Mori, Department of Radiology, Johns Hopkins University, Baltimore, Md) was used for tensor calculations (6,10). All source images from the DT imaging data sets were visually inspected by one author (T.O.), and images with visually apparent artifacts due to bulk motion were removed. In our DT imaging data set, there was low eddy current–related

Published online before print
10.1148/radiol.2382042192

Radiology 2006; 238:668–678

Abbreviations:
DT = diffusion tensor
ROI = region of interest

Author contributions:
Guarantors of integrity of entire study, T.O., Y.M., K.T.; study concepts/study design or data acquisition or data analysis/interpretation, all authors; manuscript drafting or manuscript revision for important intellectual content, all authors; approval of final version of submitted manuscript, all authors; literature research, T.O., Y.M., Y.F., H.F., M.H., K.T.; clinical studies, T.O., Y.M., Y.F., T.H., M.K., A.Y., S.U., K.T.; statistical analysis, T.O., Y.M., M.K., A.Y., M.H., K.T.; and manuscript editing, all authors

Address correspondence to Y.M.
(e-mail: *mikiy@kuhp.kyoto-u.ac.jp*).

Authors stated no financial relationship to disclose.

geometric distortion between images obtained in each motion-probing gradient direction (23,25), so postprocessing distortion correction was not applied for this data set. After calculating the six independent elements of the 3 × 3 tensor and diagonalization, three eigenvalues and three eigenvectors were obtained (1,3–5). The eigenvector associated with the largest eigenvalue was assumed to represent the intravoxel fiber orientation. The fractional anisotropy map and directional color-coded map were synthesized (Fig 1). Fiber orientations were assigned specific colors on the color-coded map, as follows: Red represented the right-to-left orientation; green, the anterior-to-posterior orientation; and blue, the superior-to-inferior orientation (26).

Fiber Tractography

The DtiStudio software was used to also perform fiber tractography on the basis of the fiber assignments derived by means of the continuous tracking method (6,9,10). With this software, tracking from all the pixels inside the brain (ie, with the brute force approach) was performed, and tracking results that penetrated the two manually segmented regions of interest (ROIs) on the basis of the known anatomic distributions of tracts were assigned to specific tracts (ie, with the two-ROI approach). Propagation in each fiber tract was terminated if a voxel with a fractional anisotropy value of less than 0.2 was reached or if the inner product of two consecutive vectors was greater than 0.75. These conditions prohibited the turning of angles larger than 41° during tracking (10).

Four fiber bundles—the corticospinal tract, the superior longitudinal fasciculus, the corticocortical connection fibers through the corpus callosum, and the limbic fibers through the fornix—were reconstructed by drawing specific ROIs according to the anatomic distributions of each fiber tract. ROI manipulations were performed by one neuroradiologist (A.Y.) with 3 years of experience performing tractography and 10 years of experience as a neuroradiologist. This author was blinded as to whether the images had been obtained by using 3.0 T or 1.5 T when he performed each ROI segmentation.

For corticospinal tract tractography, two ROIs were placed on transverse non–diffusion-weighted (b = 0 sec/mm^2) images (10,12,15) according to established anatomic landmarks: The first ROI was placed in the cerebral peduncle bilaterally, and the second ROI was placed in the precentral gyrus bilaterally (27) (Fig 2a).

The superior longitudinal fasciculus was reconstructed at tractography by placing two ROIs in the cerebral deep white matter on a coronal directional color-coded map. The superior longitudinal fasciculus was identified on the coronal color-coded map as a region where the fiber orientation was anterior to posterior (green), lateral to the corona radiata (26,28). An anterior ROI was placed in the plane passing through the reconstructed corticospinal tract, and a posterior ROI was placed in the plane passing through the rostral surface of the splenium of the corpus callosum, with both ROIs covering the green area representing the superior longitudinal fasciculus (Fig 2c). Some "noise" fibers that were apparently tracing the error course were then removed (10).

Corpus callosum tractography was performed by imaging the combination of four different callosal fiber bundles. The primary ROI was placed in the corpus callosum in the midsagittal plane (Fig 2d). To visualize different parts of the callosal fibers, secondary ROIs were placed in four regions: two ROIs on the coronal color-coded map and two ROIs on the transverse color-coded map (Fig 2e). Anterior callosal fibers, referred to as minor forceps, were reconstructed by placing the ROI covering the deep white matter in the coronal plane anterior to the genu of the corpus callosum. For reconstruction of the posterior cal-

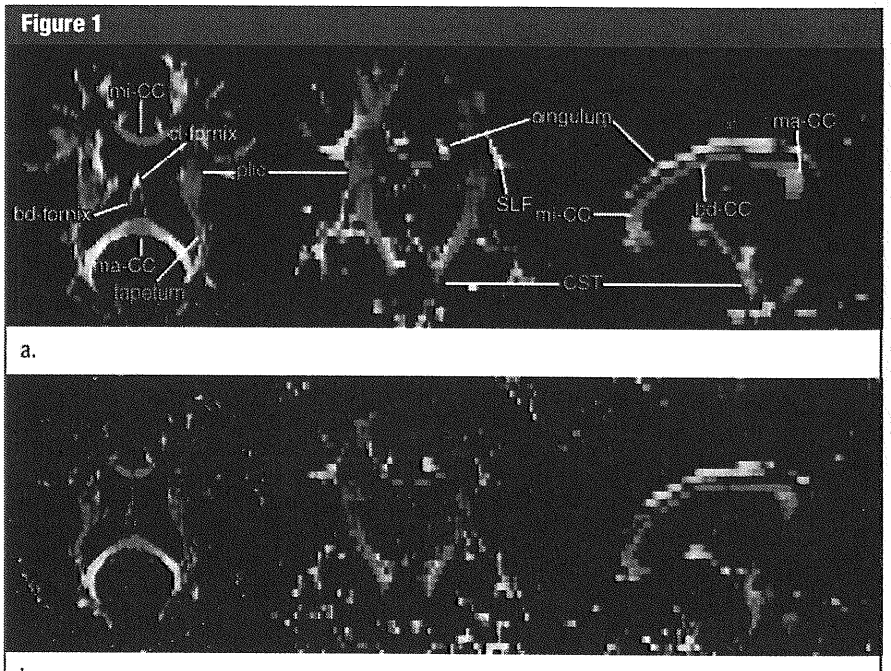

Figure 1: Transverse (left), coronal (middle), and sagittal (right) **(a)** 3.0-T and **(b)** 1.5-T color-coded maps reconstructed at DT tractography in the same subject. Red, green, and blue areas represent fibers running in right-to-left, anterior-to-posterior, and superior-to-inferior orientations, respectively. Locations of examined white matter tracts were assigned by using the 3.0-T color-coded maps. *bd-CC* = body of corpus callosum, *bd-fornix* = body of fornix, *cl-fornix* = column of fornix, *CST* = corticospinal tract, *ma-CC* = major forceps, *mi-CC* = minor forceps, *plic* = posterior limb of internal capsule (including the corticospinal tract), *SLF* = superior longitudinal fasciculus.

Figure 2

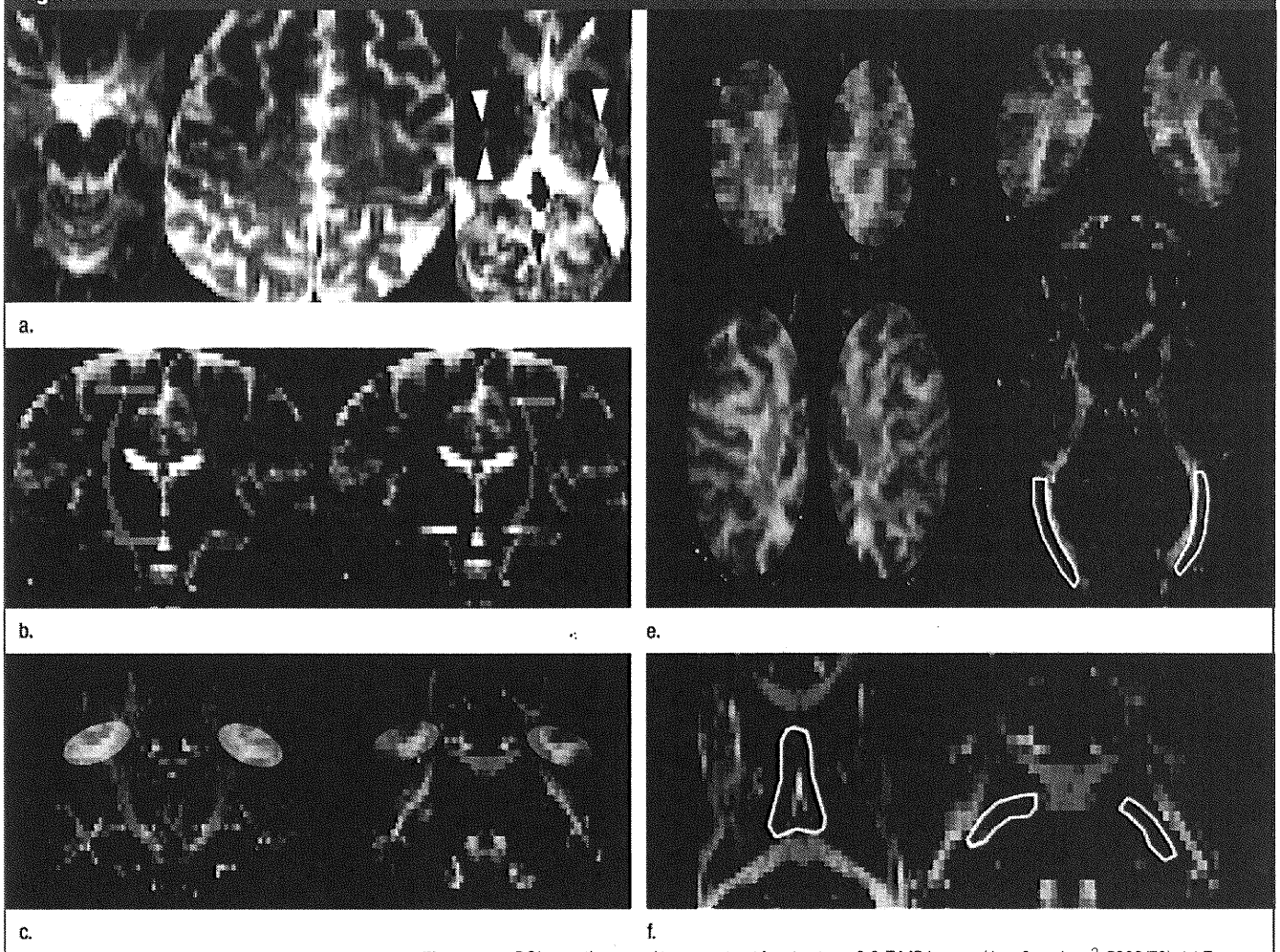

Figure 2: ROI operations used to reconstruct four tracts on 3.0-T MR images ($b = 0$ sec/mm^2, 5200/79). **(a)** Transverse images at bilateral cerebral peduncles (right), precentral gyri (middle), and internal capsule (left) show ROIs in red. Corticospinal tract is area of prolonged T2 relaxation at posterolateral aspect of internal capsule (arrowheads). **(b)** Coronal images of corticospinal tracts (red) reconstructed with cut operation. Only fibers between the ROIs (blue) were reconstructed for the right and left sides separately. **(c)** Coronal color-coded maps with ROIs (white ellipses). Anterior (left) and posterior (right) ROIs contain superior longitudinal fasciculus (green area lateral to corona radiata). **(d)** Primary ROI placed in corpus callosum on sagittal color-coded map. Vertical (coronal planes) and horizontal (transverse planes) white lines indicate section locations of secondary ROIs: anterior coronal section for minor forceps, posterior coronal for major forceps, superior transverse for body of corpus callosum, and inferior transverse for tapetum. **(e)** Transverse color-coded maps show secondary ROIs for corpus callosum: anterior ROIs for minor forceps (top left), posterior ROIs for major forceps (top right), superior ROIs for body of corpus callosum (bottom left), and inferior ROIs (white outlines) for tapetum (bottom right). **(f)** Transverse (left) and coronal (right) color-coded maps show ROIs (white outlines) for fornix. Primary (superior) ROI was placed at body of fornix (left); secondary (posterior) ROIs, at crura of fornices bilaterally (right).

losal fibers, referred to as major forceps, the ROI was placed posterior to the splenium of the corpus callosum. Callosal body fibers were reconstructed by placing the ROI at the centrum semiovale in the transverse plane superior to the body of the corpus callosum. For reconstruction of the temporal interhemispheric connection fibers, referred to as tapetum, ROIs were placed bilaterally in the temporal deep white matter, lateral to the trigon of the lateral ventricles. These four fibers (ie, minor forceps, major forceps, callosal body fibers, and tapetum) were combined to delineate the entire corpus callosum.

Limbic fibers through the fornix were reconstructed by placing one primary ROI and two secondary ROIs. The primary ROI was placed in the body of the fornix, and the secondary ROIs

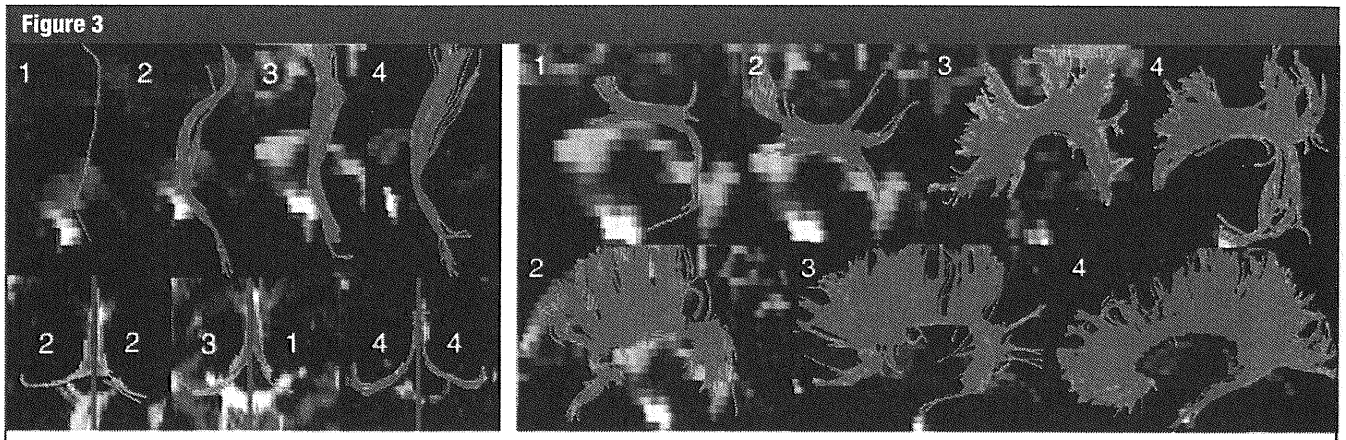

Figure 3: Scoring (scores *1–4*) for fiber tract depiction at tractography. Red areas represent the depicted tracts. **(a)** Top: Corticospinal tractographic image superimposed on sagittal non–diffusion-weighted images (5200/79) viewed from left side. Grades *1* and *2* were assigned at 1.5-T imaging, and grades *3* and *4* were assigned at 3.0-T imaging. Bottom: Fornix tractographic image obtained at 3.0 T superimposed on transverse non–diffusion-weighted images (5200/79). Blue lines separate right and left fornix tractographic images. **(b)** Superior longitudinal fasciculus tractographic image (top) and corpus callosum tractographic image (bottom) superimposed on sagittal non–diffusion-weighted images (5200/79) viewed from left side. For superior longitudinal fasciculus tractography (top), grades 1 and 2 were assigned at 1.5-T imaging, and grades 3 and 4 were assigned at 3.0-T imaging. For corpus callosum tractography, grade 2 was assigned at 1.5 T imaging, and grades 3 and 4 were assigned at 3.0-T imaging. In no subject was grade 1 assigned at corpus callosum tractography.

were placed in the crura of the right and left fornices anterolateral to the splenium of the corpus callosum (Fig 2f).

Evaluation of Tractography

The tractographic depiction of fiber tracts was graded on three-dimensional volume views and in three orthogonal two-dimensional planes by two neuroradiologists (T.O., with 2 years of experience performing tractography; Y.M., with 3 years of experience performing tractography and 19 years of experience as a neuroradiologist). Grading was performed on the basis of the following three criteria: the fiber tract volume, the anatomic distribution of the tract, and the presence or absence of the tract at the expected location. The readers were blinded to the magnetic field strength used (1.5 or 3.0 T). After performing independent interpretations, the two readers resolved any score discrepancies by consensus to establish final scores.

One score was derived from one tractographic examination—not from the pair of ROIs used to perform reconstructing tractography. The scores assigned at fiber tractography were as follows: 4 meant excellent—that is, the depicted fiber tract accurately matched the known anatomic distribution, and there was a sufficient volume of fibers; 3 meant adequate for diagnosis—that is, imaging errors such as image distortion and tract propagation error were minor, so the image was still adequate for use as a diagnostic tool; 2 meant fair—that is, moderate imaging errors or moderate tract volume loss markedly reduced imaging quality; 1 meant poor—that is, there were major imaging errors and/or tract volume loss, and the readers were unable to interpret the course or shape of the tract; and 0 meant no tract visualization.

At corticospinal tract tractography, anatomically accurately depicted tracts were defined as those passing through the lateral segment of the cerebral peduncle, the posterior limb of the internal capsule, and the precentral gyrus. At superior longitudinal fasciculus tractography, fibers connecting the frontal and parietal lobes (ie, long association fibers) and fibers connecting the frontal and temporal lobes (ie, arcuate fibers) were considered. Anatomically accurate results for the superior longitudinal fasciculus were defined as good visualization of both the long association fibers and the arcuate fibers. At corpus callosum tractography, anatomically accurate results were defined as good visualization of the four different subsegments. At limbic tractography, the depiction of fibers connecting the column, body, and crus of the fornix was considered to represent anatomically accurate results. At tractography, the depicted superior longitudinal fasciculus, corpus callosum, and fornix are each composed of several subsegments of fiber bundles, and all subsegments were integrated to establish a single final score for each tractographic examination. The scoring of tractographic images is illustrated in Figure 3.

Tractographic depictions of the corticospinal tract, superior longitudinal fasciculus, and fornix on the right and left sides were assessed independently. At corpus callosum tractography, the right and left sides were assessed together, because callosal fiber connects the right and left hemispheres.

Reconstructed tract fibers were counted by using the DtiStudio software. The numbers of fibers depicted at tractography of the corticospinal tract and the superior longitudinal fasciculus in the right and left hemispheres were counted separately. The right and left fibers were not counted separately at tractography of the corpus callosum and

the fornix, because right- and left-hemisphere limbic fibers were difficult to differentiate at the column of the fornix, which was visualized as a single fiber bundle.

Although the diffusion characteristics of the normal brain are somewhat asymmetric, corticospinal tract tractography in healthy subjects reportedly reveals minimal asymmetry (17,29). To assess the reliability of corticospinal tract tractography in healthy subjects, lateral asymmetry was evaluated on the basis of the numbers of right- and left-hemisphere fibers at tractography of the corticospinal tract. For this purpose, the "cut" operation was performed by using DtiStudio software. With the cut operation, only the fiber coordinates between the two ROIs are reconstructed (Fig 2b). The conventional two-ROI approach involves the use of three corticospinal tract regions at tractography: the areas below the cerebral peduncle, between the two ROIs, and above the precentral gyrus. These three regions have very different properties. In the region between the two ROIs, tracking results do not branch and are more robust against noise. This approach is particularly useful for quantitative analysis.

The index of asymmetry (AI) between the right *(R)* and left *(L)* corticospinal tracts in each subject at tractography was calculated as the absolute difference in fiber numbers between the two sides, divided by the mean of the two sides, as modified from a previously described method (14): $AI = L - R / [(L + R)/2]$. Lateral asymmetry analysis of superior longitudinal fasciculus tractography was not performed, because the superior longitudinal fasciculus comprises numerous long and short connecting fibers and lateral asymmetry is commonly observed in healthy subjects (6,29).

Statistical Analyses

Differences between 3.0- and 1.5-T DT imaging were calculated in terms of the following features: *(a)* depiction scores for right and left corticospinal tract tractography, right and left superior longitudinal fasciculus tractography, corpus callosum tractography, and right and left fornix tractography; *(b)* numbers of fibers depicted at right and left tractography of the corticospinal tract, right and left tractography of the superior longitudinal fasciculus, corpus callosum tractography, and fornix tractography; and *(c)* asymmetry index at corticospinal tract tractography. Statistical

Figure 4

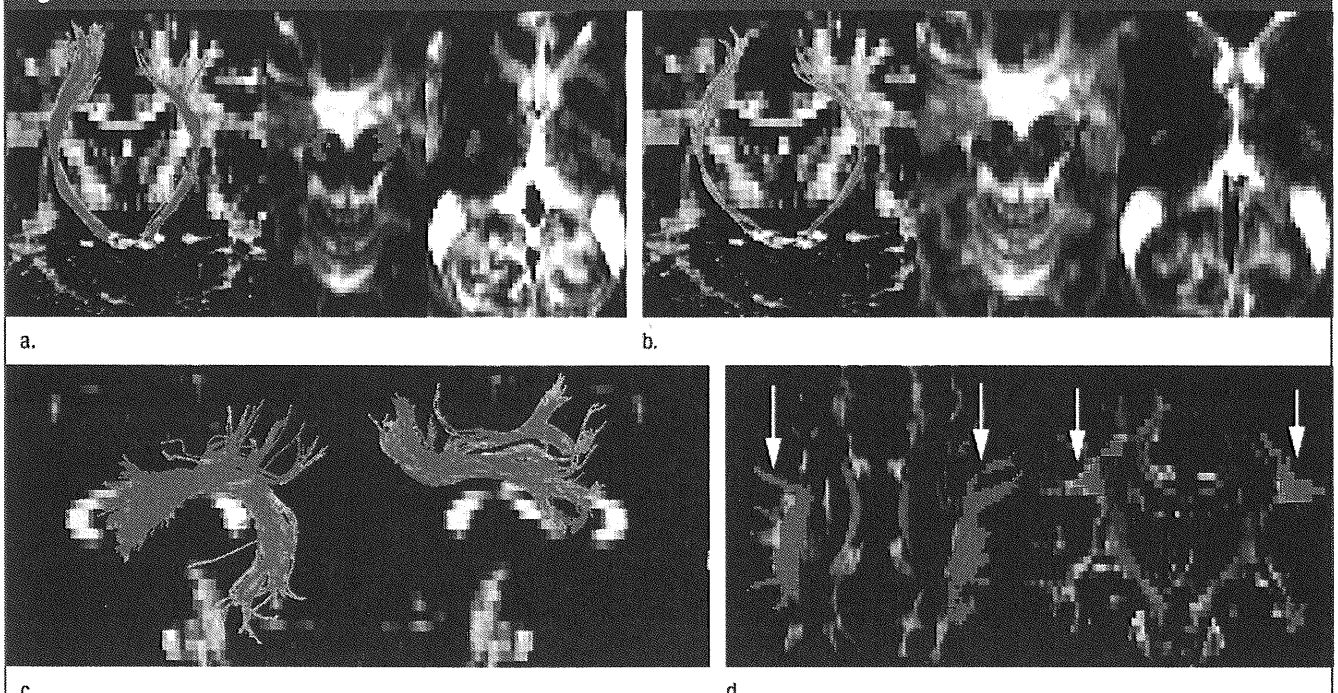

Figure 4: Fiber tractographic results. **(a, b)** Left: Three-dimensional reconstruction of corticospinal tract (red) in the same subject at **(a)** 3.0-T and **(b)** 1.5-T tractography, with use of transverse and coronal fractional anisotropy images. Middle and right: Transverse non–diffusion-weighted images with two-dimensional overlays of tractographic images at the sections of the cerebral peduncles (middle) and internal capsule (right) bilaterally. The voxels where the depicted corticospinal tract penetrates the transverse planes are shaded red. At 1.5-T corticospinal tract tractography (**b**), although the proper anatomic distribution is depicted, the tract volume is lower than that at 3.0 T. **(c)** Three-dimensional reconstruction of superior longitudinal fasciculus (red) on sagittal fractional anisotropy map at 3.0-T tractography in a different subject. At tractography in this subject, the shapes and distributions of the right and left superior longitudinal fasciculi differed. Although tractography of the left superior longitudinal fasciculus depicted arcuate fibers toward the temporal lobe, tractography of the right superior longitudinal fasciculus depicted no arcuate fibers. The corticocortical long connection fibers between the frontal and parietal lobes, however, were thicker on the right side than on the left side. **(d)** Tractographic image of superior longitudinal fasciculus (red, arrows) overlaid on 3.0-T transverse (left) and coronal (right) color-coded maps obtained in the subject described in **c** *(Fig 4 continues).*

analysis was based on the consensus scores for each tract in each subject derived by the two neuroradiologists. The Wilcoxon signed rank test was applied by using JMP, version 5.1, software (SAS Institute, Cary, NC). For all statistical analyses, $P < .05$ was considered to be indicative of a significant difference.

Results

Fiber Tract Visualization

DT imaging at both 3.0 and 1.5 T was successfully performed in all 30 subjects. The corticospinal tract was visualized at 3.0 and 1.5 T (Fig 4a, 4b) in all subjects. At superior longitudinal fasciculus tractography, long association fibers were visualized in all subjects at 3.0 and 1.5 T. Right arcuate fibers were visualized in 22 subjects (73%) at 3.0 T and in 20 subjects (67%) at 1.5 T, whereas left arcuate fibers were identified in 29 subjects (97%) at 3.0 and 1.5 T (Fig 4c, 4d).

All four subsegments of the corpus callosum were successfully visualized at 3.0 and 1.5 T (Fig 4e) in every subject. The body and column of the fornix were visualized at 3.0 and 1.5 T in every subject. The right crus of the fornix was visualized in 21 subjects (70%) at 3.0 T and in 18 subjects (60%) at 1.5 T. The left crus of the fornix was visualized in 27 subjects (90%) at 3.0 T and in 25 subjects (83%) at 1.5 T (Fig 4f). One subject was incidentally found to have cavum septum pellucidum and cavum vergae. The right and left columns of the fornix were visualized separately in this subject (Fig 4g).

All tractographic results were included in the analysis of tract depiction scores and numbers of depicted tract fibers. All tractographic results for the corticospinal tract were included for asymmetry analysis. With regard to the 420 depiction scores (30 subjects times seven tracts times two readers), there were discrepancies between the two independent readers regarding 152 scores (36%). The two readers discussed the discrepancy and established a final consensus score in each case. The depicted fiber tracts and the depiction scores are listed in Table 1.

Statistical Analyses

For tractography of the corticospinal tract, both right- and left-hemisphere depiction scores ($P < .001$) and numbers of tract fibers (right, $P = .008$; left, $P < .001$) were significantly higher at 3.0 T than at 1.5 T. The asymmetry index at corticospinal tract tractography was significantly lower at 3 T ($P < .001$). For tractography of the right su-

Figure 4

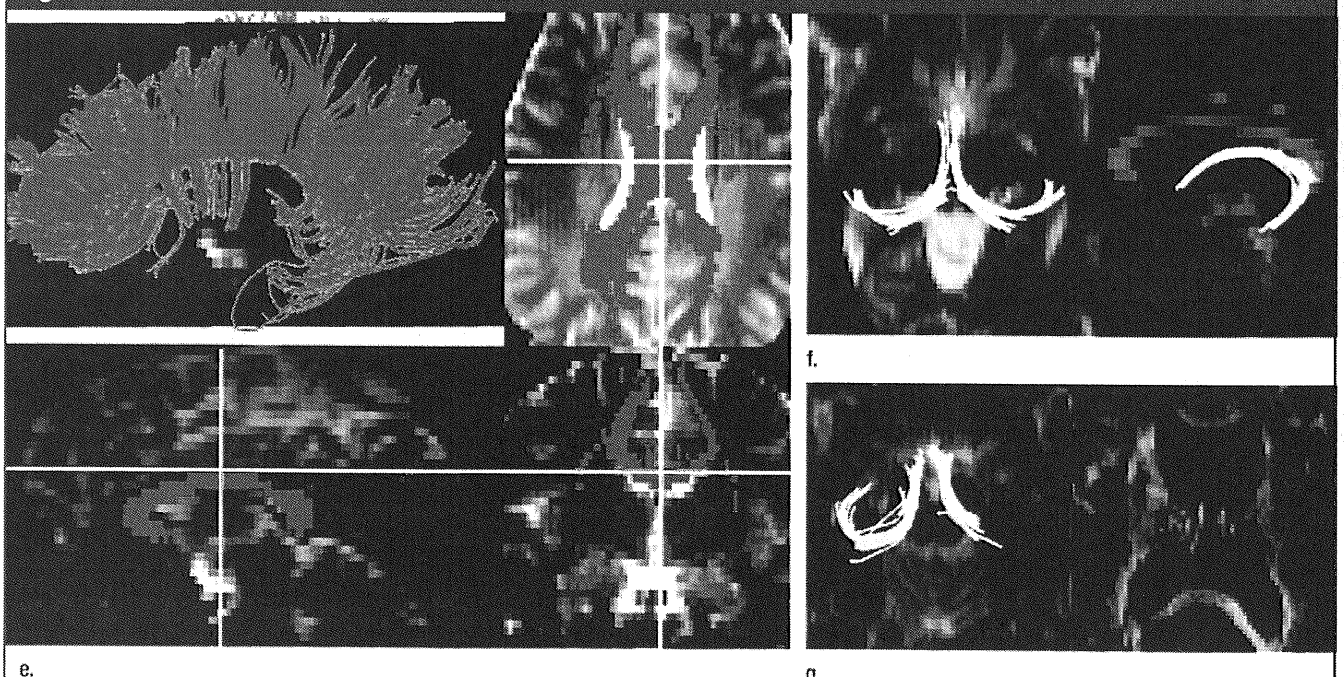

Figure 4 *(continued)*: **(e)** Three-dimensional 3.0-T tractographic reconstruction of corpus callosum (red) on sagittal non–diffusion-weighted image (5200/79) (top left) and on overlay in three orthogonal planes (top right, bottom left, and bottom right). Various kinds of transcallosal connection fibers are depicted. The center indicated by the intersecting of the vertical and horizontal lines on the three orthogonal images (top right, bottom left, and bottom right) indicate the same location. **(f)** Three-dimensional 3.0-T tractographic reconstruction of fornix (yellow) on transverse non–diffusion-weighted image (5200/79) (left) and sagittal color-coded map viewed from left (right). **(g)** Three-dimensional 3.0-T tractographic reconstruction of fornix (yellow) on transverse non–diffusion-weighted image (5200/79) (left) and transverse color-coded map (right) obtained in a subject with cavum septum pellucidum and cavum vergae. The bodies and columns of the fornices on the right and left sides were visualized separately.

perior longitudinal fasciculus, depiction scores (P = .005) and numbers of tract fibers (P = .001) were significantly higher at 3.0 T than at 1.5 T. Depiction scores for tractography of the left superior longitudinal fasciculus did not differ significantly between 3.0- and 1.5-T DT imaging. For tractography of the left superior longitudinal fasciculus, the numbers of tract fibers were significantly higher at 3.0 T than at 1.5 T (P = .02). For corpus callosum tractography, depiction scores were significantly higher at 3.0 T than at 1.5 T (P = .01), although the numbers of tract fibers did not differ significantly. Scores for depiction of the right fornix (P = .04) and numbers of fornix tract fibers bilaterally (P = .02) were significantly higher at 3.0 T than at 1.5 T, although scores for depiction of the left fornix were not significantly different. These results are summarized in Table 2.

Table 1

Depiction Scores Assigned at Fiber Tractography

Tract and Score	3.0-T Tractography	1.5-T Tractography
Right corticospinal tract		
0	0	0
1	0	2
2	1	8
3	6	13
4	23	7
Left corticospinal tract		
0	0	0
1	0	6
2	1	9
3	6	10
4	23	5
Right superior longitudinal fasciculus		
0	0	0
1	1	3
2	10	11
3	6	9
4	13	7
Left superior longitudinal fasciculus		
0	0	0
1	1	0
2	3	3
3	14	17
4	12	10
Corpus callosum		
0	0	0
1	0	0
2	2	6
3	9	14
4	19	10
Right fornix		
0	0	0
1	10	11
2	8	16
3	11	3
4	1	0
Left fornix		
0	0	0
1	3	4
2	14	17
3	12	9
4	1	0

Note.—Data are numbers of subjects with the given depiction score. Scores were determined in consensus between two readers.

Discussion

In recent studies, investigators have reported on intraindividual comparisons between 3.0- and 1.5-T DT imaging performed for functional MR imaging based on blood oxygen level–dependent contrast (30), intracranial time-of-flight MR angiography (31), supraaortic contrast material–enhanced MR angiography (32), and high-spatial-resolution inner ear imaging (33). These studies revealed the clinical feasibility of and the better visualization that is achievable at 3.0-T imaging compared with these features at 1.5-T imaging. DT imaging also reportedly yields a higher signal-to-noise ratio at 3.0 T, suggesting the possibility that it renders higher spatial resolution without enhanced noise-related errors (22,34).

Parallel imaging techniques involve the use of multiple receiver coil elements for spatial information encoding and gradient encoding and, owing to shortened echo train lengths, have been shown to markedly reduce the number of echo-planar imaging–related artifacts. The potential of parallel imaging for DT imaging has been demonstrated at both 1.5 and 3.0 T (21,22). Naganawa et al (23) challenged the optimization of 3.0-T DT fiber tractography performed with parallel imaging and found that DT imaging data on brain fiber tracking in healthy subjects can be acquired within a very short imaging time (<2 minutes). Nagae-Poetscher et al (24) performed high-spatial-resolution DT imaging of the brainstem at 3.0 T with parallel imaging and visualized various brainstem structures, including deep cerebellar nuclei, some cranial nerves, and white matter tracts.

To our knowledge, our study is the first in which the findings of 3.0- and